

# Synthesis of $^{13}\text{C}$ -depleted organic matter from CO in a reducing early Martian atmosphere

Received: 21 March 2023

Accepted: 5 April 2024

Published online: 09 May 2024

 Check for updates

Yuichiro Ueno <sup>1,2,3</sup>✉, Johan A. Schmidt <sup>4,9</sup>, Matthew S. Johnson <sup>4</sup>, Xiaofeng Zang <sup>1</sup>, Alexis Gilbert <sup>1,2</sup>, Hiroyuki Kurokawa <sup>2,5</sup>, Tomohiro Usui <sup>2,6</sup> & Shohei Aoki <sup>7,8</sup>

Organic matter found in early Martian sediment may yield clues to the planet's environmental conditions, prebiotic chemistry and habitability, but its origin remains unclear. Strong  $^{13}\text{C}$  depletion in sedimentary organic matter at Gale crater was recently detected by the Curiosity rover. Although this enigmatic depletion remains debated, if correct, a mechanism to cause such strong  $^{13}\text{C}$  depletion is required. Here we show from  $\text{CO}_2$  photolysis experiments and theoretical considerations that solar ultraviolet photolysis of  $\text{CO}_2$  in a reducing atmosphere can yield strongly  $^{13}\text{C}$ -depleted CO. We suggest that atmospheric synthesis of organic compounds from photolysis-produced CO is a plausible mechanism to explain the source of isotopically depleted organic matter in early Martian sediments. Furthermore, this mechanism could explain  $^{13}\text{C}$  enrichment of early Martian  $\text{CO}_2$  without requiring long-term carbon escape into space. A mass balance model calculation using our estimated isotopic fractionation factor indicates the conversion of approximately 20% of volcanic  $\text{CO}_2$  emissions on early Mars into organics via CO, consistent with the available data for carbon isotopes of carbonate. Although alternative pathways for organic compound production have been proposed, our findings suggest that considerable amounts of organic matter may have been synthesized from CO in a reducing early Martian atmosphere and deposited in sediments.

Organic matter on Mars is important for understanding the habitability of the planet, prebiotic chemistry and the search for life in the universe. A series of analyses using the Sample Analysis at Mars (SAM) instrument on board the Curiosity rover discovered and confirmed that there is sedimentary organic matter preserved in circa

3.5-billion-year-old water-lain sediment at the Gale crater on Mars<sup>1–4</sup>. Furthermore, recent analysis of SAM data revealed that this organic matter has an enigmatic stable carbon isotope composition ( $\delta^{13}\text{C}_{\text{VPDB}}$  values [ $\equiv 1000((^{13}\text{C}/^{12}\text{C})_{\text{sample}}/(^{13}\text{C}/^{12}\text{C})_{\text{VPDB}} - 1)$ ] from  $-137\text{‰}$  to  $+22\text{‰}$ ) (refs. 5–9), some of which are strongly depleted in  $^{13}\text{C}$  to an extent never

<sup>1</sup>Department of Earth and Planetary Sciences, Tokyo Institute of Technology, Tokyo, Japan. <sup>2</sup>Earth-Life Science Institute, Tokyo Institute of Technology, Tokyo, Japan. <sup>3</sup>Japan Agency for Marine-Earth Science and Technology (JAMSTEC), Yokosuka, Japan. <sup>4</sup>Department of Chemistry, University of Copenhagen, Copenhagen, Denmark. <sup>5</sup>Department of Earth Science and Astronomy, Graduate School of Arts and Sciences, The University of Tokyo, Tokyo, Japan. <sup>6</sup>Institute of Space and Astronautical Science, Japan Aerospace Exploration Agency, Kanagawa, Japan. <sup>7</sup>Department of Complexity Science and Engineering, Graduate School of Frontier Sciences, The University of Tokyo, Kashiwa, Japan. <sup>8</sup>Royal Belgian Institute for Space Aeronomy, Brussels, Belgium. <sup>9</sup>Present address: Devlabs ApS, Copenhagen, Denmark. ✉ e-mail: [ueno.y.ac@m.titech.ac.jp](mailto:ueno.y.ac@m.titech.ac.jp)

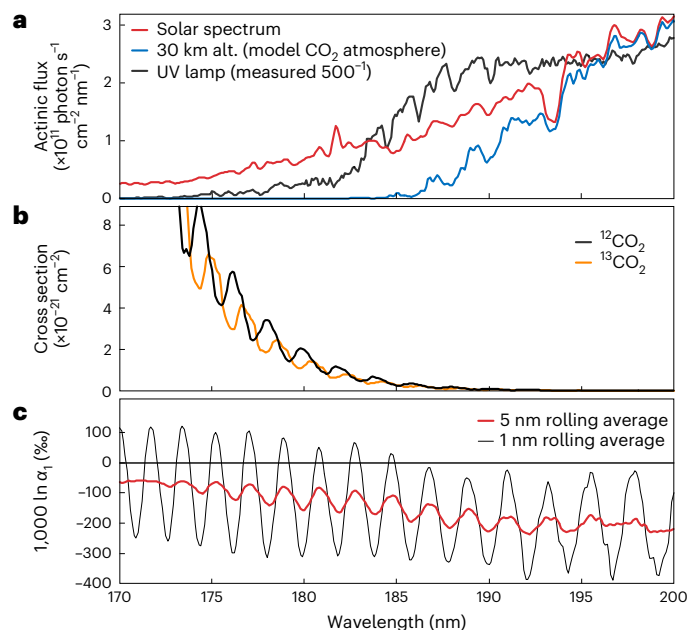


**Fig. 1 | Wavelength-dependent isotopic fractionation of CO<sub>2</sub> photolysis.**

Preferential dissociation of <sup>12</sup>CO<sub>2</sub> against <sup>13</sup>CO<sub>2</sub> is expected in a wavelength region from 170 nm to 200 nm, which is responsible for solar UV photolysis of CO<sub>2</sub>.

**a**, Actinic UV spectra. Red: solar spectrum from ref. 43. Blue: calculated spectrum at 30 km altitude (alt.) of model early Mars (10 mbar CO<sub>2</sub> at surface) (Methods). Black: measured UV spectrum of the high pressure Xe lamp used in the laboratory experiment (Methods). **b**, Calculated absorption cross sections of <sup>12</sup>CO<sub>2</sub> (black) and <sup>13</sup>CO<sub>2</sub> (orange) at 295 K from ref. 17. **c**, Calculated isotope effect (1,000 ln α<sub>1</sub>) as a function of wavelength for the 295 K absorption spectra. Results were averaged over a 1 nm (black) and 5 nm (red) windows. Oxygen isotopic fractionation and its implications for Mars atmosphere were given elsewhere<sup>17</sup>.

found in Earth's sedimentary rocks<sup>6</sup>. Although some in situ isotope analyses have been contaminated by a terrestrial material mixed into the SAM instrument<sup>3–10</sup>, even taking this into account, it appears that several early Martian sediments contain organic carbon with δ<sup>13</sup>C<sub>VPDB</sub> values at least less than –70‰ (ref. 10) and possibly down to –137 ± 8‰ (refs. 6, 8) (Supplementary Note provide details).

The origin of this strong <sup>13</sup>C depletion remains uncertain but may arise from cosmic, biological or abiological processes<sup>4–6</sup>. Interplanetary dust may include carbon particles with strong <sup>13</sup>C depletion<sup>11</sup> and might have accumulated in the sediment<sup>6</sup>, although the signal from outside the solar system would easily be diluted if indigenous carbon sources were available from biotic or abiotic processes on Mars. Some biological metabolic pathways, particularly methanotrophy, can induce large isotopic fractionation, but it is difficult to explain δ<sup>13</sup>C<sub>VPDB</sub> < –100‰ in light of known biological fractionation factors<sup>6</sup>. In principle, the organic matter in early Martian sediment could be due to abiotic reactions such as Fischer–Tropsch-type reactions<sup>2,6</sup> or electro-chemical reduction of CO<sub>2</sub><sup>5,6,12</sup>, but none of these mechanisms are known to produce the large carbon isotopic fractionations observed (ref. 6 and references therein). An alternative source of organic matter is atmospheric synthesis<sup>5,6,13–16</sup>. Theoretically, atmospheric photochemistry under the appropriate conditions may produce a large carbon isotopic fractionation<sup>14,15,17</sup>. Ab initio calculations using time-dependent wavepacket propagation of the absorption cross sections of CO<sub>2</sub> isotopologues<sup>17</sup> predicted that solar UV photolysis of CO<sub>2</sub> yields strongly <sup>13</sup>C-depleted CO, potentially lower than –100‰ (Fig. 1). However, the large isotope effect has not yet been verified by laboratory experiment<sup>17,18</sup>.

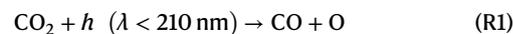
Explaining the origin of the strong <sup>13</sup>C depletion becomes even more problematic considering that the early carbonate precipitate in the approximately 4 billion years old (4 Ga) Martian meteorite ALH

84001 was rather enriched in <sup>13</sup>C (up to +55‰) (refs. 19–21) relative to Mars mantle carbon (δ<sup>13</sup>C<sub>VPDB</sub> = –25 ± 5‰) (ref. 22) (Methods). For present-day Mars, the <sup>13</sup>C enrichment of atmospheric CO<sub>2</sub> (δ<sup>13</sup>C<sub>VPDB</sub> = +46 ± 4‰) (ref. 23) has been thought to result from carbon escape into space<sup>14,24,25</sup> through the 4-billion-year history of Mars. However, even assuming the 4 Ga carbonate were in equilibrium with the atmospheric CO<sub>2</sub>, its δ<sup>13</sup>C<sub>VPDB</sub> value should have already been enriched in <sup>13</sup>C (+20 ± 10‰) at that time (Methods provide details). It is problematic to understand whether several hundred million years after formation of Martian atmosphere, enough time has passed to create the <sup>13</sup>C enrichment of CO<sub>2</sub> only via carbon escape into space<sup>14,25</sup>. Furthermore, based on geomagnetic observations<sup>26</sup>, early Mars probably had a geomagnetic field before 4 Ga. The geomagnetic field on early Mars could have prevented solar winds from interacting with ions in the upper atmosphere and shielded the neutral atmosphere from sputtering loss. Robust magnetic shielding of the atmosphere before 4 Ga is supported by observations of low-fractionated atmospheric argon (<sup>38</sup>Ar/<sup>36</sup>Ar) and nitrogen (<sup>15</sup>N/<sup>14</sup>N) recorded in ALH 84001<sup>27,28</sup>. Therefore, <sup>13</sup>C enrichment of Mars' early carbonate is still enigmatic and may have been caused by other fractionation processes<sup>14,25,29</sup>.

Here we present a new laboratory experiment and quantum theoretical and model calculations that demonstrate how solar UV photolysis of CO<sub>2</sub> and subsequent organic synthesis from atmospheric CO could explain both the strong <sup>13</sup>C depletion in the organic matter and the <sup>13</sup>C enrichment of CO<sub>2</sub>. A previous CO<sub>2</sub> photolysis experiment<sup>18</sup> was conducted using an ultraviolet light source with a confined wavelength at 184.9 nm, which does not simulate the actual fractionation that occurs in a planetary atmosphere where the expected isotope effect depends on the broad distribution of wavelengths of the actinic UV flux<sup>17</sup> (Fig. 1). Therefore, we used a solar-like broadband UV source for CO<sub>2</sub> photolysis (Fig. 1a) to confirm the large carbon isotope effect and quantify the actual fractionation factor associated with CO<sub>2</sub> photolysis in the early Martian atmospheres.

## Photolysis experiment

Our experiments demonstrated that CO<sub>2</sub> photolysis by UV from 170 to 210 nm produced highly <sup>13</sup>C-depleted CO relative to the starting CO<sub>2</sub>, with δ<sup>13</sup>C values ranging from –129‰ to –133‰ at 33 kPa CO<sub>2</sub> and approximately –122‰ at 10 kPa CO<sub>2</sub> (Fig. 2 and Extended Data Table 1). The experiment was performed under dry condition that minimizes H<sub>2</sub>O photolysis and OH chemistry (Methods) and using a light source that mimics the solar broadband UV spectrum (Fig. 1 and Extended Data Fig. 1). In our experiment, the carbon isotope fractionation originated from the following reactions:



where  $h\nu$  represents photon,  $\lambda$  denotes wavelength and  $M$  represents another molecule that acts as the collision partner. More details regarding these reactions are provided in the Methods section. Fitting of the data for the 33-kPa experiment demonstrated that the majority of fractionation was derived from reaction (R1) ( $\alpha_1 \equiv (^{13}\text{CO} / ^{12}\text{CO}) / (^{13}\text{CO}_2 / ^{12}\text{CO}_2) = 0.871 \pm 0.001$ ), whereas the isotope effect from reaction (R2) was an order of magnitude smaller ( $\alpha_2 \equiv (^{13}\text{CO}_2 / ^{12}\text{CO}_2) / (^{13}\text{CO} / ^{12}\text{CO}) = 1.0074 \pm 0.0005$ ) (Fig. 2 and Extended Data Table 2).

Theoretically, the isotopic fractionation of CO<sub>2</sub> photolysis arises from a shift in the energy and intensity of the absorption cross section of <sup>13</sup>CO<sub>2</sub> relative to <sup>12</sup>CO<sub>2</sub> (Methods and ref. 17). The fractionation changes depending on the temperature and actinic UV spectrum (Methods and Extended Data Fig. 1). To confirm the mechanism, we calculated the fractionation factor α<sub>1</sub> using the measured UV spectrum of our UV source and the ab initio cross sections calculated at 320 K,

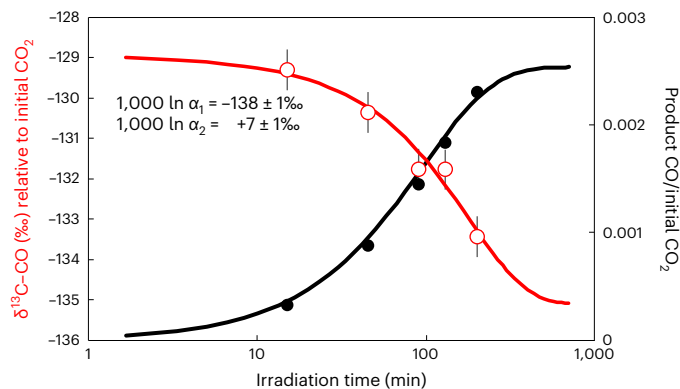


**Fig. 2 | The result of CO<sub>2</sub> photolysis experiments.** Solid circles show the CO fraction produced from CO<sub>2</sub>. Red circles show the carbon isotope composition of CO normalized against that of the initial CO<sub>2</sub> ( $\delta^{13}\text{C-CO} = ((^{13}\text{CO}/^{12}\text{CO}) / (^{13}\text{CO}_2/^{12}\text{CO}_2) - 1) \times 1,000\%$ ). Error bars represent external reproducibility (standard deviation:  $n = 10$ ) of the mass spectrometric analysis determined by replicated analysis of in-house standard CO gas. Red and black lines represent the calculated isotope ratio and CO fraction, respectively, assuming fractionation factors for CO<sub>2</sub> photolysis ( $\alpha_1 = 0.871$ ) and for CO oxidation ( $\alpha_2 = 1.0074$ ).

which correspond to the experimental conditions (Methods and Extended Data Fig. 1). As a result, the calculated effect ( $\alpha_1 = 0.845 \pm 0.004$ ;  $1,000 \ln \alpha_1 = -168 \pm 5\%$ ) is very similar to, although 30% smaller than, the observed isotope effect ( $1,000 \ln \alpha_1 = -138 \pm 1\%$ ) (details are provided in Methods and Extended Data Fig. 1). On the basis of the sensitivity analysis for temperature and potential spectral changes due to attenuation by O<sub>2</sub> and CO<sub>2</sub> (Methods and Extended Data Fig. 1), we conclude that the systematic 30% difference probably arises from the accuracy of the ab initio calculation for the theoretical CO<sub>2</sub> potential energy surface<sup>17</sup> rather than uncertainties in the experiment. Therefore, fractionations calculated using the theoretical cross sections of Schmidt et al.<sup>17</sup> may be overestimated by approximately 30%. Nonetheless, our analysis confirms that the broadband solar UV photolysis of CO<sub>2</sub> is associated with a large negative carbon isotope effect ( $1,000 \ln \alpha < -100\%$ ). This is also supported by satellite observations showing strong <sup>13</sup>C depletion of CO in Earth's mesosphere<sup>30</sup> and in the present-day lower atmosphere of Mars<sup>31–33</sup>, where photolysis of CO<sub>2</sub> is the main source of CO.

## Isotopic fractionation in an early Martian atmosphere

In the early Martian atmosphere, the actual isotopic fractionation by CO<sub>2</sub> photolysis may have been even larger than that observed in our experiment (Extended Data Figs. 2 and 3). After applying the correction determined by the experiment, the actual fractionation factor  $\alpha_1$  was calculated for the modelled 1D early Mars atmospheres at different  $P_{\text{CO}_2}$  and temperature profiles (Methods and Extended Data Figs. 2 and 3). The effective fractionation between the starting CO<sub>2</sub> and product CO is at least 60% greater in the simulations than in the experiment at 320 K (Table 1). This is generally because lower temperatures lead to larger isotopic fractionation ( $-0.8\%$  K<sup>-1</sup>) owing to the contribution of vibrational hot bands to the absorption cross sections of CO<sub>2</sub> isotopologues. In addition, higher  $P_{\text{CO}_2}$  gives slightly larger fractionation because photons in shorter-wavelength regions (<190 nm) are selectively attenuated by CO<sub>2</sub> itself (Fig. 1 and Extended Data Figs. 2 and 3). The fractionation at the surface may be larger by approximately 100% than at 100 km in altitude, although the effect of  $P_{\text{CO}_2}$  on the overall fractionation is small for the total column (only a 20% difference between 10 mbar and 100 mbar  $P_{\text{CO}_2}$  cases). Therefore, temperature is the most important factor controlling the magnitude of the isotope effect.

**Table 1 | Calculated isotope effect of CO<sub>2</sub> photolysis for modelled early Mars atmospheres**

Surface temperature (K)	$P_{\text{CO}_2}$ at surface (mbar)	Fractionation factor: $\alpha$	Isotope effect: $1,000 \ln \alpha$ (‰) (total column)	Isotope effect: $1,000 \ln \alpha$ (‰) (below 60 km)
300	10	0.8106	-210	-220
300	100	0.7890	-237	-245
240	10	0.7766	-253	-264
240	100	0.7615	-273	-276

Detailed assumptions for the calculations are provided in Methods.

Whereas the temperature profile of the early Martian atmosphere is uncertain, the surface temperature should have been near the freezing point of water (273 K) when the organics were deposited in water-lain sediment under the presence of liquid water. On the other hand, some geomorphological studies of the early Martian sediments suggest glacial conditions<sup>6,34</sup>, implying that the surface temperature did not greatly exceed 273 K. Therefore, it is reasonable to assume a surface temperature less than 300 K, which gives a calculated global average  $\delta^{13}\text{C}$  value of CO lower than  $-210\%$  (Table 1, Fig. 3 and Extended Data Figs. 2 and 3). The large carbon isotopic fractionation from the solar UV photolysis of CO<sub>2</sub> induces a strong <sup>13</sup>C depletion in CO in the early Martian atmosphere (Fig. 3).

## Atmospheric synthesis of organic matter from CO

Under reducing atmospheric conditions, CO can be converted into simple organic compounds, mainly formaldehyde and possibly methanol<sup>13,35</sup>. In addition to aldehydes, our recent experiments demonstrated that atmospheric CO can generate carboxylic acids, mainly formate and acetate<sup>16</sup>. In the atmosphere, all these soluble organics are incorporated into water and probably rained out. Even starting from pure CO<sub>2</sub>, these organic compounds are produced via CO when H<sub>2</sub> in the atmosphere scavenges excess OH radicals produced by the photolysis of H<sub>2</sub>O<sup>13–16</sup>. In such a reducing environment, the photolysis of CO<sub>2</sub> is a key rate-limiting step for the atmospheric synthesis of organic compounds via CO (Methods). If the early Martian atmosphere was reducing<sup>14,36–38</sup>, then the strongly <sup>13</sup>C-depleted CO would transfer into soluble organics and then deposit into the sediment. Therefore, atmospheric synthesis from CO could explain the origin of organics, with strong <sup>13</sup>C depletion, observed in early Martian sediments (Fig. 3).

Conversely, the CO<sub>2</sub> remaining after photolysis should be enriched in <sup>13</sup>C owing to the conservation of mass (Rayleigh fractionation process), unless the product CO is oxidized quantitatively back into CO<sub>2</sub> (Fig. 3) (Methods). Therefore, the isotopic ratio of CO<sub>2</sub> is useful for constraining the carbon cycling in the early Martian atmosphere. Using the experimental fractionation factor determined in the present study ( $\alpha_1 = 0.871$ ), a simple mass balance calculation (Fig. 3a) shows that an approximate 30% conversion of CO<sub>2</sub> into CO results in a  $-140\%$  of  $\delta^{13}\text{C}_{\text{VPDB}}$  value for CO, as reported for Martian organics, and gives  $+20\%$  for the remaining CO<sub>2</sub>, which is consistent with the estimated atmospheric CO<sub>2</sub> from the 4-Ga Martian meteorite. Note that the estimated 30% conversion could be seen as an upper bound because the model does not consider atmospheric escape. Nonetheless, this result implies that CO<sub>2</sub> photolysis can explain the <sup>13</sup>C enrichment of atmospheric CO<sub>2</sub> relative to the Martian mantle ( $\delta^{13}\text{C}_{\text{VPDB}} = -25 \pm 5\%$ ; Methods provides the estimate), even if we do not consider carbon escape into space.

However, in the case of early Mars, atmospheric CO may not have been derived solely from CO<sub>2</sub> photolysis but also directly from volcanism because CO could be a major carbon species in volcanic gas along with CO<sub>2</sub> owing to the reducing conditions in the Mars mantle<sup>38–41</sup>. Starting from a 90:10 mixture of volcanic CO<sub>2</sub>:CO and using the experimental fractionation factor determined in the present study ( $\alpha_1 = 0.8106$ ) for modelled early Mars (Fig. 3b), an approximately 20% conversion of CO<sub>2</sub>

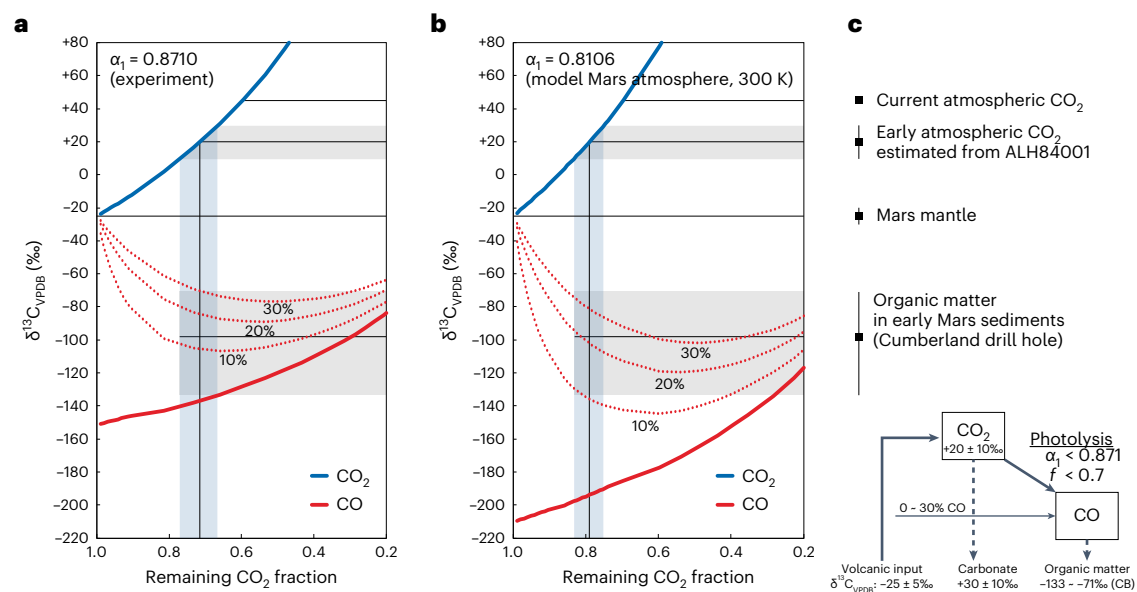


**Fig. 3 | Modelled global averaged carbon isotopic compositions of atmospheric CO<sub>2</sub> and CO on early Mars.** **a**,  $\delta^{13}\text{C}_{\text{VPDB}}$  values of CO<sub>2</sub> (blue) and CO (red) as a function of the remaining CO<sub>2</sub> after photolysis ( $f = (\text{CO}_2) / (\text{CO}_2 + \text{CO})$ ), assuming the experimental fractionation factor ( $\alpha_1 = 0.871$ ). Dotted lines show the cases for volcanic gas containing 10%, 20% and 30% CO, which has the same  $\delta^{13}\text{C}_{\text{VPDB}}$  value as volcanic CO<sub>2</sub> ( $-25 \pm 5\%$  (ref. 22)). **b**, The model assuming

fractionation factor ( $\alpha_1 = 0.8106$ ) calculated for model Mars atmosphere (Methods). **c**, Reported carbon isotope ratios used for constraining the model (Methods). The possible ranges of  $\delta^{13}\text{C}_{\text{VPDB}}$  values for early atmospheric CO<sub>2</sub> and organic matter in Cumberland (CB) drill core are also shown in **a** and **b**.

into CO results in a  $\delta^{13}\text{C}_{\text{VPDB}}$  value of  $-135\%$  for the produced CO and  $+20\%$  for the remaining CO<sub>2</sub>. Our simple model calculation also indicates that the observed  $^{13}\text{C}$  depletion and large isotopic heterogeneity ( $-137\%$  to  $-70\%$ ) (ref. 6) in several early Martian sediments could be produced when organics are synthesized from CO not only produced by CO<sub>2</sub> photolysis but also from volcanic CO (Fig. 3c).

Organics from CO in the atmosphere may not have been a single source for the Martian sedimentary organic matter. Potentially, other sources<sup>2,5,6,12</sup> may have provided more  $^{13}\text{C}$ -rich organics from CO<sub>2</sub> and diluted the signal of the strong  $^{13}\text{C}$  depletion. Note that the measured  $\delta^{13}\text{C}_{\text{VPDB}}$  values for the organic matter in early Martian sediments are very heterogeneous with values ranging from  $-137\%$  to  $+22\%$  (refs. 5–10), which may suggest multiple sources (Supplementary Note). Isotopically heavier CO<sub>2</sub> could have been incorporated into the organics if the carboxylation reaction occurred before or after precipitation. After deposition, the aldehydes and other organics could have been condensed into larger molecules through Formose-type reactions<sup>42</sup>, though post-depositional processes are largely unknown in the early Mars environment.

In any case, our experimental results and theoretical and model calculations demonstrate that solar UV photolysis of CO<sub>2</sub> is a plausible origin of the observed  $^{13}\text{C}$  depletion of sedimentary organic matter in early Martian sediment and the  $^{13}\text{C}$  enrichment of the 4-Ga carbonate. The mass balance model suggests that an appreciable amount of organic matter would have been synthesized via CO in a reducing early Martian atmosphere and stored in early Martian sediments. These results do not preclude a biological origin for the Martian organic matter, although they imply that atmospheric synthesis could be quantitatively more important for producing organics on early Mars.

## Online content

Any methods, additional references, Nature Portfolio reporting summaries, source data, extended data, supplementary information, acknowledgements, peer review information; details of author contributions and competing interests; and statements of data and code availability are available at <https://doi.org/10.1038/s41561-024-01443-z>.

## References

- Ming, D. W. et al. Volatile and organic compositions of sedimentary rocks in Yellowknife Bay, Gale Crater, Mars. *Science* **15**, 343 (2014).
- Freissinet, C. et al. Organic molecules in the Sheepbed Mudstone, Gale Crater, Mars. *J. Geophys. Res. Planets* **120**, 495–514 (2015).
- Eigenbrode, J. L. et al. Organic matter preserved in 3-billion-year-old mudstones at Gale Crater, Mars. *Science* **360**, 1096–1101 (2018).
- Millan, M. et al. Sedimentary organics in Glen Torridon, Gale Crater, Mars: results from the SAM instrument suite and supporting laboratory analyses. *J. Geophys. Res. Planets* **127**, e2021JE007107 (2021).
- Franz, H. B. et al. Indigenous and exogenous organics and surface-atmosphere cycling inferred from carbon and oxygen isotopes at Gale Crater. *Nat. Astron.* **4**, 526–532 (2020).
- House, C. H. et al. Depleted carbon isotope compositions observed at Gale Crater, Mars. *Proc. Natl Acad. Sci. USA* **119**, e2115651119 (2022).
- Schoell, M. Methane  $^{13}\text{C}/^{12}\text{C}$  isotope analyses with the SAM-EGA pyrolysis instrument suite on Mars Curiosity rover: a critical assessment. *Proc. Natl Acad. Sci. USA* **119**, e2205344119 (2022).
- House, C. H. et al. Reply to Schoell: implications of a temperature trend in methane evolved from Cumberland during Mars evolved gas analyses experiments. *Proc. Natl Acad. Sci. USA* **119**, e2207901119 (2022).
- Stern, J. C. et al. Organic carbon concentrations in 3.5-billion-year-old lacustrine mudstones of Mars. *Proc. Natl Acad. Sci. USA* **119**, e2201139119 (2022).
- Peters, K. & Schoell, M.  $^{13}\text{C}$ -depleted methane pyrolyzed from contaminated Gale Crater sediment cores, Mars. *Icarus* **410**, 115890 (2024).
- Sakai, N., Saruwatari, O., Sakai, T., Takano, S. & Yamamoto, S. Abundance anomaly of the  $^{13}\text{C}$  species of CCH. *Astron. Astro Phys.* **512**, A31 (2010).

12. Steele, A. et al. Organic synthesis associated with serpentinization and carbonation on early Mars. *Science* **375**, 172–177 (2022).
13. Pinto, J. P., Gladstone, G. R. & Yung, Y. L. Photochemical production of formaldehyde in Earth's primitive atmosphere. *Science* **210**, 183–185 (1980).
14. Lammer, H. et al. Loss and fractionation of noble gas isotopes and moderately volatile elements from planetary embryos and early Venus, Earth and Mars. *Space Sci. Rev.* **216**, 74 (2020).
15. Stüeken, E. E. et al. Mission to planet Earth: the first two billion years. *Space Sci. Rev.* **216**, 31 (2020).
16. Zang, X., Ueno, Y. & Kitadai, N. Photochemical synthesis of ammonia and amino acids from nitrous oxide. *Astrobiology* **22**, 387–398 (2022).
17. Schmidt, J. A., Johnson, M. S. & Schinke, R. Carbon dioxide photolysis from 150 to 210 nm: singlet and triplet channel dynamics, UV-spectrum, and isotope effects. *Proc. Natl Acad. Sci. USA* **110**, 17691–17696 (2013).
18. Bhattacharya, S. K., Savarino, J. & Thieme, M. H. A new class of oxygen isotopic fractionation in photodissociation of carbon dioxide: potential implications for atmospheres of Mars and Earth. *Geophys. Res. Lett.* **27**, 1459–1462 (2000).
19. Niles, P. B., Leshin, L. A. & Guan, Y. Microscale carbon isotope variability in ALH84001 carbonates and a discussion of possible formation environments. *Geochim. Cosmochim. Acta* **69**, 2931–2944 (2005).
20. Halevy, I., Fischer, W. W. & Eiler, J. M. Carbonates in the Martian meteorite Allan Hills 84001 formed at  $18 \pm 4^\circ\text{C}$  in a near-surface aqueous environment. *Proc. Natl Acad. Sci. USA* **108**, 16895–16899 (2011).
21. Shaheen, R., Niles, P. B., Chong, K., Corrigan, C. M. & Thieme, M. H. Carbonate formation events in ALH 84001 trace the evolution of the Martian atmosphere. *Proc. Natl Acad. Sci. USA* **112**, 336–341 (2015).
22. Wright, I. P., Grady, M. M. & Pillinger, C. T. Chassigny and the Nakhilites: carbon-bearing components and their relationship to martian environmental conditions. *Geochim. Cosmochim. Acta* **56**, 817–826 (1992).
23. Webster, C. R. et al. Isotope ratios of H, C, and O in CO<sub>2</sub> and H<sub>2</sub>O of the Martian atmosphere. *Science* **341**, 260–263 (2013).
24. Jakosky, B. M., Pepin, R. O., Johnson, R. E. & Fox, J. L. Mars atmospheric loss and isotopic fractionation by solar-wind-induced sputtering and photochemical escape. *Icarus* **111**, 271–288 (1994).
25. Hu, R., Kass, D. M., Ehlmann, B. L. & Yung, Y. L. Tracing the fate of carbon and the atmospheric evolution of Mars. *Nat. Commun.* **6**, 10003 (2015).
26. Lillis, R. J., Robbins, S., Manga, M., Halekas, J. S. & Frey, H. V. Time history of the Martian dynamo from crater magnetic field analysis. *J. Geophys. Res. Planets* **118**, 1488–1511 (2013).
27. Mathew, K. J. & Marti, K. Early evolution of Martian volatiles: nitrogen and noble gas components in ALH84001 and Chassigny. *J. Geophys. Res.* **106**, 1401–1422 (2001).
28. Kurokawa, H., Kurosawa, K. & Usui, T. A lower limit of atmospheric pressure on early Mars inferred from nitrogen and argon isotopic compositions. *Icarus* **299**, 443–459 (2018).
29. Galimov, E. On the phenomenon of enrichment of Mars in <sup>13</sup>C: a suggestion on the reduced initial atmosphere. *Icarus* **147**, 472–476 (2000).
30. Beale, C. A., Buzan, E. M., Boone, C. D. & Bernath, P. F. Near-global distribution of CO isotopic fractionation in the Earth's atmosphere. *J. Mol. Spectrosc.* **323**, 59–66 (2016).
31. Yoshida, T. et al. Strong depletion of <sup>13</sup>C in CO induced by photolysis of CO<sub>2</sub> in the Martian atmosphere calculated by a photochemical model. *Planet. Sci. J.* **4**, 53 (2023).
32. Aoki, S. et al. Strong depletion of <sup>13</sup>C in CO in the atmosphere of Mars revealed by ExoMars-TGO/NOMAD. *Planet. Sci. J.* **4**, 97 (2023).
33. Alday, J. et al. Photochemical depletion of heavy CO isotopes in the Martian atmosphere. *Nat. Astron.* **7**, 867–876 (2023).
34. Head, J. W. III, Marchant, D. R. & Ghatan, G. J. Glacial deposits on the rim of a Hesperian-Amazonian outflow channel source trough: Mangala Valles, Mars. *Geophys. Res. Lett.* **31**, L10701 (2004).
35. Bar-Nun, A. & Chang, S. Photochemical reactions of water and carbon monoxide in Earth's primitive atmosphere. *J. Geophys. Res.* **88**, 6662–6672 (1983).
36. Zahnle, K., Haberle, R. M., Catling, D. C. & Kasting, J. F. Photochemical instability of the ancient Martian atmosphere. *J. Geophys. Res.* **113**, E11004 (2008).
37. Haberle, R. M., Zahnle, K., Barlow, N. G. & Steakley, K. E. Impact degassing of H<sub>2</sub> on early Mars and its effect on the climate system. *Geophys. Res. Lett.* **46**, 13355–13362 (2019).
38. Sholes, S. F., Smith, M. L., Claire, M. W., Zahnle, K. J. & Catling, D. C. Anoxic atmospheres on Mars driven by volcanism: implications for past environments and life. *Icarus* **290**, 46–62 (2017).
39. Zolotov, M. Y. & Shock, E. L. A thermodynamic assessment of the potential synthesis of condensed hydrocarbons during cooling and dilution of volcanic gases. *J. Geophys. Res.* **105**, 539–559 (2000).
40. Gaillard, F. & Scaillet, B. A theoretical framework for volcanic degassing chemistry in a comparative planetology perspective and implications for planetary atmospheres. *Earth Planet. Sci. Lett.* **403**, 307–316 (2014).
41. Yung, Y. L. et al. Methane on Mars and habitability: challenges and responses. *Astrobiology* **18**, 1221–1242 (2018).
42. Kim, H. J. et al. Synthesis of carbohydrates in mineral-guided prebiotic cycles. *J. Am. Chem. Soc.* **133**, 9457–9468 (2011).
43. Rottman, G. J., Woods, T. N. & McClintock, W. SORCE solar UV irradiance results. *Adv. Space Res.* **37**, 201–208 (2006).

**Publisher's note** Springer Nature remains neutral with regard to jurisdictional claims in published maps and institutional affiliations.

**Open Access** This article is licensed under a Creative Commons Attribution 4.0 International License, which permits use, sharing, adaptation, distribution and reproduction in any medium or format, as long as you give appropriate credit to the original author(s) and the source, provide a link to the Creative Commons licence, and indicate if changes were made. The images or other third party material in this article are included in the article's Creative Commons licence, unless indicated otherwise in a credit line to the material. If material is not included in the article's Creative Commons licence and your intended use is not permitted by statutory regulation or exceeds the permitted use, you will need to obtain permission directly from the copyright holder. To view a copy of this licence, visit <http://creativecommons.org/licenses/by/4.0/>.

© The Author(s) 2024

## Methods

### CO<sub>2</sub> photolysis experiment

Photolysis experiments were carried out in a glass flask apparatus with a UV-grade synthetic quartz window used in ref. 16. The diameter of the UV window was 3.6 cm. The volume of the apparatus was 448 cm<sup>3</sup>, and maximum path length was 13 cm. A Xenon arc lamp (Cermax, CX-04E, PE300BUV) was used as the UV source. The actinic UV spectrum was measured by a vacuum UV monochromator system<sup>44</sup> (Extended Data Fig. 1), which was used for calculating theoretical fractionation factor for the CO<sub>2</sub> photolysis.

Before the experiment, the glass flask was evacuated to below 0.1 Pa for more than 12 h. After evacuation, high-purity CO<sub>2</sub> (>99.99995%, Japan Air Gases) was introduced into the flask through the vacuum line to avoid contamination with air. The total gas pressure in the flask was measured using a capacitance manometer (MKS Baratron 626 B, 1–10 kPa range).

UV irradiation was performed at an output power of 20 A for the Xe lamp. The temperature of the flask was maintained at 315 ± 5 K using a cooling bath (AsOne MC-1). Before and during irradiation, a small aliquot of gas in the flask was sampled by expanding it to a calibrated volume with a syringe port. Each sample contained 1.7% of the total gas in the flask.

### Carbon isotope analysis

The carbon isotopic composition of CO was measured using gas chromatography-combustion-isotope ratio mass spectrometry. The sampled gas was first purified by gas chromatography (Trace GC Ultra, Thermo Fisher Scientific) equipped with a capillary column (HP-MOLSIEVE:30 m × 0.53 mm i.d., 25 μm film thickness; Varian) to separate N<sub>2</sub>, O<sub>2</sub>, CO, CH<sub>4</sub> and CO<sub>2</sub>. Ultra-high-purity He (>99.99995%, Japan Air Gases) was used as the carrier gas. The gas chromatography (GC) oven was maintained at 50 °C with a flow rate of 1.5 ml min<sup>-1</sup>. After the analysis, the GC temperature was raised to 200 °C to remove any remaining gases in the column. Purified CO was then converted into CO<sub>2</sub> at 1,100 °C in a combustion furnace consisting of a ceramic tube packed with CuO, NiO and Pt wires. Then, CO<sub>2</sub> was introduced into an isotope ratio mass spectrometer (MAT253, Thermo Fisher Scientific) via the combustion furnace and continuous flow interface (GC Combustion III, Thermo Fisher Scientific). Isotopic standardization was performed using CO<sub>2</sub> injections calibrated against the National Institute of Standards and Technology natural gas standard, NGS-2.

Carbon isotope ratio is reported using the delta notation:

$$\delta^{13}\text{C} - \text{CO} = \left( \frac{{}^{13}\text{R}_{\text{CO}}}{{}^{13}\text{R}_{\text{CO}_2}} - 1 \right) \times 1,000 \text{‰}$$

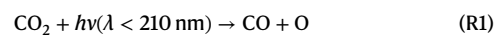
where <sup>13</sup>R<sub>CO</sub> and <sup>13</sup>R<sub>CO<sub>2</sub></sub> represent <sup>13</sup>C/<sup>12</sup>C ratios of the sampled CO and the initial CO<sub>2</sub> used in the experiment, respectively. The initial CO<sub>2</sub> used in the photolysis experiment was also measured using GC-isotope ratio mass spectrometry (IRMS), as described in ref. 45. On the basis of replicated analyses of the samples and in-house standard CO gas, the reproducibility of the measured δ<sup>13</sup>C–CO value was better than ±0.5‰. All the experimental results are summarized in Extended Data Tables 1 and 2.

### Theoretical calculation for absorption cross sections for <sup>12</sup>CO<sub>2</sub> and <sup>13</sup>CO<sub>2</sub>

The absorption cross sections for <sup>12</sup>C<sup>16</sup>O<sup>16</sup>O, <sup>13</sup>C<sup>16</sup>O<sup>16</sup>O and three other isotopologues of CO<sub>2</sub> were calculated from first principles using a time-dependent quantum mechanical methodology. The calculations were based on potential energy surfaces for the ground and lower excited states of CO<sub>2</sub>, which were calculated using the multireference configuration interaction plus the Davidson correction to correlation energy (MRCI + Q) quantum chemistry method (ref. 17 provides details). The absorption cross sections for <sup>12</sup>C<sup>16</sup>O<sup>16</sup>O, <sup>13</sup>C<sup>16</sup>O<sup>16</sup>O, and three other isotopologues of CO<sub>2</sub> between 120 K and 395 K are available in the supporting information of ref. 17, in which Dataset S1 is for <sup>12</sup>C<sup>16</sup>O<sup>16</sup>O, S2 is for <sup>12</sup>C<sup>16</sup>O<sup>17</sup>O, S3 is for <sup>12</sup>C<sup>16</sup>O<sup>18</sup>O, S4 is <sup>13</sup>C<sup>16</sup>O<sup>16</sup>O and S5 is for <sup>13</sup>C<sup>16</sup>O<sup>18</sup>O.

### Calculation of the fractionation factor for CO<sub>2</sub> photolysis in the experiment

In the CO<sub>2</sub> photolysis experiment, carbon isotope fractionation potentially originates from the following two reactions:



where *M* represents the third-body reaction partner. The reaction rates of reactions (R1) and (R2) are proportional to the number densities of CO<sub>2</sub> and CO and thus can be written as *J*[CO<sub>2</sub>] and *k*[CO], respectively. In our experiment, more than 99.7% of CO<sub>2</sub> remained in the system, and thus the reaction rate of reaction (R1) (that is, *J*[CO<sub>2</sub>]) was constant, whereas the reaction rate of (R2) (that is, *k*[CO]) increased in response to elevated [CO] (Fig. 2). In this case, the isotopic fractionation factors for (R1) and (R2) are defined as

$$\alpha_1 = {}^{13}J/{}^{12}J \quad (1)$$

$$\alpha_2 = {}^{13}k'/{}^{12}k' \quad (2)$$

where <sup>12</sup>*J* and <sup>13</sup>*J* are the photolysis rate coefficients of <sup>12</sup>CO<sub>2</sub> and <sup>13</sup>CO<sub>2</sub>, respectively. In addition, <sup>12</sup>*k*' and <sup>13</sup>*k*' are the rate constants for <sup>12</sup>CO and <sup>13</sup>CO, respectively. The *J*, *k*, *α*<sub>1</sub> and *α*<sub>2</sub> values were estimated by fitting the observed changes in CO / (CO + CO<sub>2</sub>) and δ<sup>13</sup>C–CO (Fig. 2).

For the 33-kPa experiment (Extended Data Table 1), the best fit values for *J* and *k*' were 4.3 × 10<sup>-7</sup> s<sup>-1</sup> and 1.7 × 10<sup>-4</sup> s<sup>-1</sup>, respectively. The steady-state CO/CO<sub>2</sub> ratio (= *J* / *k*') was 0.0025. In reality, a longer experiment yields O<sub>2</sub> via the following reaction.



When O<sub>2</sub> accumulates in the system, the simple assumptions above are no longer applicable owing to the more complex O<sub>2</sub> photochemistry and UV shielding by O<sub>2</sub>, both of which should affect the *k*' and *J* values. Therefore, we report the data only before O<sub>2</sub> accumulated in the system (up to 4 h under our experimental conditions).

In addition, the same model simulation was performed by splitting the *J* and *k* values into those for <sup>12</sup>C and <sup>13</sup>C species by assuming fractionation factors *α*<sub>1</sub> and *α*<sub>2</sub>. For the 33-kPa experiment (Extended Data Table 1), the best fit values for *α*<sub>1</sub> and *α*<sub>2</sub> were 0.871 ± 0.001 and 1.0074 ± 0.0005, respectively. Consequently, the observed isotope fractionation (δ<sup>13</sup>C–CO from –133‰ to –121‰) is largely due to the isotope effect of CO<sub>2</sub> photolysis (1,000 ln *α*<sub>1</sub> = –138 ± 1‰) with a smaller contribution from reaction (R2) (1,000 ln *α*<sub>2</sub> = +7.4 ± 0.5‰).

To confirm the small isotope effect of reaction (R2), additional experiments were performed, in which the reaction rate of reaction (R2) was enhanced by adding O<sub>2</sub> (Extended Data Table 2). In this experiment, a 1:2:8 mixture of CO:O<sub>2</sub>:N<sub>2</sub> was photolysed using the same UV source. After 345 min, 30% of the initial CO was consumed via reaction (R2). The remaining CO showed a relatively large scatter in its δ<sup>13</sup>C value (±4.4‰; *n* = 8) and did not show a significant correlation with the remaining CO fraction. These results confirmed that the isotope effect of reaction (R2) should be smaller than ±13‰ when considering a possible ±4.4‰ change at 30% consumption. This is consistent with the estimated +7.4 ± 0.5‰ isotope effect for reaction (R2).

In an actual atmosphere, photolysis generates oxygen atoms (O), although the direct recombination of CO with O to give CO<sub>2</sub> is forbidden by the conservation of spin and is therefore very slow, allowing quantitative amount of CO to build up<sup>46</sup>. The excess oxygen is removed by the oxidation of surface minerals or escapes into space, and the atmosphere overall could be weakly reducing.

Also, in actual atmosphere, presence of H<sub>2</sub>O may change the photochemistry relative to our dry experimental condition. Photodissociation of H<sub>2</sub>O creates the OH radical, which is the dominant oxidant of CO. Therefore, in wet conditions, CO oxidation rate is faster than in a dry atmosphere<sup>13–16</sup>. On the other hand, the presence of H<sub>2</sub>O does not change the fractionation factor of CO<sub>2</sub> photolysis ( $\alpha_1$ ) unless water vapour considerably modifies the actinic UV spectra. The spectral effect is evaluated in the following sections.

### Comparison to theoretical fractionation factor in the experimental condition

The observed large isotope effect in CO<sub>2</sub> photolysis ( $\alpha_1 = 0.871 \pm 0.001$ ;  $1,000 \ln \alpha_1 = -138 \pm 1\%$ ) was compared with theoretical calculations to obtain a mechanistic understanding of this effect. Theoretically, the isotopic fractionation factor for CO<sub>2</sub> photolysis ( $\alpha_1$ ) can be calculated using equation (1) and absorption cross sections for CO<sub>2</sub> isotopologues<sup>17</sup>

$$^{12}J = \int_{170}^{210} \varphi(\lambda)^{12} \sigma(\lambda) I(\lambda) e^{-\tau(\lambda)} d\lambda \quad (3)$$

$$^{13}J = \int_{170}^{210} \varphi(\lambda)^{13} \sigma(\lambda) I(\lambda) e^{-\tau(\lambda)} d\lambda \quad (4)$$

where  $^{12}J$  and  $^{13}J$  represent the photolysis rate coefficients of  $^{12}\text{CO}_2$  and  $^{13}\text{CO}_2$ , respectively.  $\varphi(\lambda)$  is the quantum yield, which is assumed to be unity in the integral range from 170 nm to 210 nm.  $^{12}\sigma(\lambda)$  and  $^{13}\sigma(\lambda)$  are absorption cross sections at a wavelength  $\lambda$  for  $^{12}\text{CO}_2$  and  $^{13}\text{CO}_2$ , respectively, as reported in ref. 17.  $I(\lambda)$  is the incident UV spectrum in our experimental condition, measured by the vacuum UV monochromator used in ref. 35 (Extended Data Fig. 1). The opacity term  $\tau(\lambda)$  was calculated as follows:

$$\tau(\lambda) = \sum_i \sigma_i \int \rho_i(z) dz \quad (5)$$

where  $\sigma_i(\lambda)$  is the absorption cross section of the UV-shielding molecule  $i$  and  $\int \rho_i(z) dz$  represents the column density of molecule  $i$  in path length  $z$ . The gases defining the opacity term should have large cross sections in the 170–210 nm wavelength range. Potentially, the presence of O<sub>2</sub> and CO<sub>2</sub> (self shielding) can change the actinic UV flux, thereby changing the fractionation factor  $\alpha_1$ .

The calculation results are summarized in Extended Data Fig. 1. First, the actinic UV spectra did not change considerably from the front and rear ends of the 13-cm-long apparatus (Extended Data Fig. 1). CO<sub>2</sub> self shielding may shift the isotope effect ( $1,000 \ln \alpha_1$ ) by up to  $-1\%$  for 33-kPa CO<sub>2</sub> and by a negligible amount for 10 kPa CO<sub>2</sub> (Extended Data Fig. 1). UV shielding by O<sub>2</sub> may possibly cause a larger shift of up to  $-4\%$ , even considering an improbably high O<sub>2</sub> content (100 Pa; Extended Data Fig. 1). In our experiment, O<sub>2</sub> was formed by reaction (R3), although its concentration was probably lower than that of CO (maximum 70 Pa; Extended Data Table 1). Conservatively, we take  $\pm 4\%$  as the error derived from the uncertainty of the UV spectrum.

The uncertainty arising from temperature may cause a larger variation. Although our UV experiment started at 297 K, the temperature increased to  $315 \pm 5$  K after 10 min. The heating of the apparatus was inevitable in the current experimental setting. On the other hand, the ab initio cross sections for the CO<sub>2</sub> isotopologues change slightly depending on temperature<sup>17</sup>. Using the cross sections at 295 K, the estimated isotope effect ( $1,000 \ln \alpha_1$ ) was 9.4% larger than that using 320 K cross sections (Extended Data Fig. 1). We found that a lower temperature resulted in larger fractionation (in other words, a more negative  $1,000 \ln \alpha_1$  value) with a slope of  $+0.51\% \text{ K}^{-1}$  from 220 K to 320 K.

Considering the above uncertainties, the theoretical fractionation factor  $\alpha_1$  for our experimental condition (33 kPa CO<sub>2</sub>) was  $0.845 \pm 0.004$ , corresponding to  $-168 \pm 5\%$  for  $1,000 \ln \alpha_1$ , which was 30% more negative than the observed isotope effect of  $-138 \pm 1\%$ .

The systematic 30% difference may not be due to uncertainties in the UV experiment, but are more likely due to inaccuracies in the ab initio potential energy surfaces used to calculate the theoretical CO<sub>2</sub> cross sections. Precise calculations in the lower energy region of the absorption cross section are particularly difficult. On the basis of the  $^{12}J$  and  $^{13}J$  spectra (Extended Data Fig. 1), the lower energy part (that is  $\lambda > 183$  nm) is the main region giving rise to large fractionation. Considering the difficulty of the calculation, a conservative estimate of the error in the ab initio cross sections is  $\pm 50\%$ , which is similar to the theoretical fractionations calculated for similar gases, including nitrous oxide (N<sub>2</sub>O)<sup>47</sup> and carbonyl sulfide (OCS)<sup>48</sup>. Therefore, we estimate that the experimentally determined isotope effect ( $-138 \pm 1\%$ ) is consistent with the theoretical fractionation within an uncertainty of  $\pm 50\%$ . Note that calculated fractionation using theoretical cross sections<sup>17</sup> overestimates fractionation by 30% relative to the experiment. The ab initio calculation and the experiment confirm our hypothesis that broadband UV photolysis of CO<sub>2</sub> is associated with a large negative carbon isotope effect in excess of  $-100\%$ .

### Estimated fractionation factor for CO<sub>2</sub> photolysis in the early Mars atmosphere

In the early Martian atmosphere, the isotope effect in CO<sub>2</sub> photolysis was larger than that observed in the laboratory. Considering the above fractionation mechanism, isotopic fractionation changes depending on the following key parameters:

1. Temperature
2. Actinic UV spectrum
3. UV shielding by atmospheric species

All three of these factors from the early Mars were different from the experimental conditions and are not precisely known. Therefore, we built a 1D atmospheric simulation model to help understand the sensitivity and error.

The base model assumed a hydrostatic CO<sub>2</sub> atmosphere with 10 mbar  $P_{\text{CO}_2}$  at the surface (Extended Data Fig. 2a). The vertical temperature profile had a temperature of 240 K at the surface (dashed line in Extended Data Fig. 2a), which agrees with observations of the current Martian atmosphere<sup>49</sup>. A warmer case (300 K at the surface) was also calculated in the model (solid line in Extended Data Fig. 2a) to simulate early Mars with liquid water present on the surface.

The actinic UV spectra were calculated assuming the solar UV spectrum from ref. 43 and UV attenuation by CO<sub>2</sub> at each altitude (Extended Data Fig. 2d). The UV scattering by CO<sub>2</sub> was also considered using the scattering cross section from ref. 50.

The photolysis rates for  $^{12}\text{CO}_2$  and  $^{13}\text{CO}_2$  were calculated using equations (3), (4) and (5) (Extended Data Figs. 2b,e), which gives the isotopic fractionation factor ( $\alpha_1$ ) at each altitude from equation (1) (Extended Data Fig. 2c). To evaluate the temperature dependence, we used  $^{12}\text{CO}_2$  and  $^{13}\text{CO}_2$  cross sections at each temperature of the altitude profile<sup>17</sup>. A lower temperature results in a larger calculated fractionation with a slope of  $+0.8\% \text{ K}^{-1}$ , which is similar to, but slightly steeper than, that obtained under experimental conditions using a Xe lamp as a UV source ( $+0.5\% \text{ K}^{-1}$ ). Considering the systematic shift from theoretical to experimental fractionation observed, the  $1,000 \ln \alpha_1$  value was corrected with a  $+30\%$  shift across the temperature range.

### Estimated carbon isotope ratio for volcanic CO<sub>2</sub> and CO of Mars

We employed a  $\delta^{13}\text{C}$  value of  $-25 \pm 5\%$  for mantle-derived volcanic CO<sub>2</sub> and CO (Fig. 3). This value was derived from stepwise heating experiments of shergottite–nakhilite–chassignite (SNC) meteorites<sup>51</sup>. Because SNC meteorites are igneous rocks that are interpreted to represent

either lavas or plutonic cumulates<sup>52</sup>, high-temperature releases of SNC meteorites would record magmatic volatiles. The high-temperature releases (>1,000 °C) of shergottites (basalt: Shergotty and Zagami), nakhlites (clinopyroxenite: Nakhla, Lafayette, Governador Valadares) and chassignite (dunnite: Chassigny) yielded a limited  $\delta^{13}\text{C}$  range (–20‰ to –30‰), despite the fact that these meteorites have distinct formation and Mars ejection ages; that is, they were formed by different magmatic activities and were derived from different launching sites on Mars<sup>53,54</sup>. The limited  $\delta^{13}\text{C}$  values (–20‰ to –30‰) suggest the existence of a common carbon reservoir in the Martian interior.

### Estimated carbon isotope ratios for 4 Ga Mars surface water component and atmospheric CO<sub>2</sub>

We employed a  $\delta^{13}\text{C}$  value of  $+30 \pm 10\%$  for the dissolved inorganic carbon component of 4 Ga surficial water. This value is derived from –4 Ga carbonates contained in the Allan Hills (ALH) 84001 Martian meteorite<sup>19–21</sup>. ALH 84001 is an igneous cumulate (orthopyroxenite) that experienced post-magmatic aqueous alteration, resulting in the precipitation of secondary phases including carbonate<sup>55,56</sup>. Radiogenic isotope systematics (Lu–Hf, Pb–Pb and Rb–Sr) of this meteorite yield the magmatic crystallization age and the carbonate formation age of  $4.09 \pm 0.03$  Ga and  $3.9–4.0$  Ga, respectively<sup>57,58</sup>. Carbon and oxygen isotope studies indicate that carbonates were formed by distillation and loss of CO<sub>2</sub> from the fluid during evaporation and degassing<sup>20,59</sup> resulting in zoned isotopic enrichment of  $\delta^{18}\text{O}$  and  $\delta^{13}\text{C}$  from the core to the rim<sup>19,60–63</sup>. Triple oxygen isotope analyses further implied that the CO<sub>2</sub> fluid could have been initially in equilibrium with the atmosphere<sup>21,64</sup>. The  $\delta^{13}\text{C}$  value of  $+30 \pm 10\%$  employed in this study was determined to cover a reported  $\delta^{13}\text{C}$  range from 20‰ to 40‰ for Ca- and Fe-rich carbonates, which are interpreted as representing near-primary precipitates in ALH 84001 (ref. 21).

A notable feature of ALH 84001 is that the carbonates are accompanied by polycyclic aromatic hydrocarbons, nanocrystal magnetites and iron sulfides because their petrographic context and textures (for example, chain-like structure of magnetite similar to magnetotactic bacteria) invoked a possible sign of life on Mars. A question related to the biogenic origin of carbonate–magnetite–sulfide assemblages is whether they formed at a sufficiently low temperature that was suitable for life. A variety of formation temperatures from 0 °C to 650 °C have been proposed for the ALH 84001 carbonates<sup>19,20,59–63,65–68</sup>, but recent stable isotopic studies including clumped isotope geothermometry have led to a consensus that the ALH 84001 carbonates formed in a low-temperature environment (–20 °C) (for example, ref. 20). Although the low-temperature condition is consistent with both abiotic and biogenic origins, the carbonate–magnetite–sulfide assemblage in ALH 84001 is now explained as arising from abiotic processes (for example, thermal decomposition of iron carbonate due to impact-induced shock heating)<sup>69,70</sup>.

Assuming isotopic equilibrium between carbonate and atmospheric CO<sub>2</sub> ( $1,000 \ln \alpha_{\text{carbonate-CO}_2} = 9.8\%$  at 25 °C; ref. 71), we employed a  $\delta^{13}\text{C}$  value of  $+20 \pm 10\%$  for atmospheric CO<sub>2</sub> on early Mars (Fig. 3).

### Mass balance model

Carbon isotope ratios of atmospheric CO<sub>2</sub> ( $\delta^{13}\text{C}_{\text{CO}_2}$ ) and CO ( $\delta^{13}\text{C}_{\text{CO}}$ ) were calculated based on the mass balance shown in Fig. 3c. In this simple mass balance model, we assume that the atmospheric CO<sub>2</sub> arises primarily from volcanic input ( $\delta^{13}\text{C}_{\text{CO}_2-i} = -25 \pm 5\%$  as noted above) and removed as organics synthesized from CO. For simplicity, carbon isotopic fractionation ( $\alpha$ ) is assumed to occur only in the CO<sub>2</sub> photolysis. Then, isotopic compositions of atmospheric CO<sub>2</sub> is determined by remaining fraction ( $f$ ) of CO<sub>2</sub> after the photolysis:

$$\delta^{13}\text{C}_{\text{CO}_2} = (1,000 + \delta^{13}\text{C}_{\text{CO}_2-i}) \times f^{\alpha-1} - 1,000$$

Owing to mass balance:

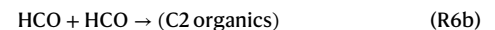
$$\delta^{13}\text{C}_{\text{CO}_2-i} = f\delta^{13}\text{C}_{\text{CO}_2} + (1-f)\delta^{13}\text{C}_{\text{org}}$$

isotopic compositions of atmospheric CO is:

$$\delta^{13}\text{C}_{\text{CO}} = (1,000 + \delta^{13}\text{C}_{\text{CO}_2-i}) \times (1-f^{\alpha}) / (1-f) - 1,000$$

In this model, we do not consider carbon escape into space, which may also cause <sup>13</sup>C enrichment of remaining CO<sub>2</sub>. Therefore, the estimated  $f$  is regarded as the maximum value if a considerable fraction of the atmospheric CO<sub>2</sub> escapes into space. In addition, molecular diffusion in the upper part of the atmosphere may also cause isotopic fractionation. However, based on our more detailed atmospheric model<sup>31</sup>, this effect is important only above 100 km altitude, which accounts for less than  $10^{-6}$  of total atmospheric CO<sub>2</sub>. Therefore, it is reasonable to neglect the isotope effect of molecular diffusion in calculating the mass balance.

Note that the model does not consider further processes that fractionate isotopes after CO<sub>2</sub> photolysis (that is,  $\alpha = \alpha_i$ ). Therefore, the isotopic composition of the organic matter ( $\delta^{13}\text{C}_{\text{org}}$ ) is equal to that of atmospheric CO ( $\delta^{13}\text{C}_{\text{CO}}$ ). This assumption may not be true if some organics were produced not from the CO but from the other carbon sources with normal or heavy isotopic composition. In a CO<sub>2</sub> and/or CO atmosphere, however, organic synthesis is initiated from the HCO radical produced by CO<sup>13,16,31,35,46,72–75</sup>.



In comparison to reaction (R1), it is very likely that carbon isotope fractionations for reactions (R4)–(R6) are an order of magnitude smaller than the CO<sub>2</sub> photolysis<sup>31,76,77</sup>. Therefore, it is reasonable to assume the strongly <sup>13</sup>C-depleted signature in CO should be transferred to formaldehyde and other organics. There is no known atmospheric reaction that incorporates the isotopically normal CO<sub>2</sub> directly into organic molecules<sup>77</sup>, unless CO<sub>2</sub> is photolysed into CO with a large isotopic fractionation (reaction (R1)). The possible alternative carbon source with normal <sup>13</sup>C abundance is volcanic CO. Therefore, we have performed additional calculations considering 10%, 20% and 30% addition of volcanic CO ( $\delta^{13}\text{C}_{\text{CO}_2-i} = -25 \pm 5\%$ ) and shown in Fig. 3.

### Data availability

The absorption cross sections for <sup>12</sup>C<sup>16</sup>O<sup>16</sup>O, <sup>13</sup>C<sup>16</sup>O<sup>16</sup>O and three other isotopologues of CO<sub>2</sub> between 120 K and 395 K are available in the supporting information of ref. 17, in which Dataset S1 is for <sup>12</sup>C<sup>16</sup>O<sup>16</sup>O, S2 is for <sup>12</sup>C<sup>16</sup>O<sup>17</sup>O, S3 is for <sup>12</sup>C<sup>16</sup>O<sup>18</sup>O, S4 is <sup>13</sup>C<sup>16</sup>O<sup>16</sup>O and S5 is for <sup>13</sup>C<sup>16</sup>O<sup>18</sup>O (<https://doi.org/10.1073/pnas.1213083110>). The datasets generated during the current study are available via Figshare at <https://doi.org/10.6084/m9.figshare.25498981> (ref. 78). Source data are provided with this paper.

### References

- Endo, Y., Ueno, Y., Aoyama, S. & Danielache, S. O. Sulfur isotope fractionation by broadband UV radiation to optically thin SO<sub>2</sub> under reducing atmosphere. *Earth Planet. Sci. Lett.* **453**, 9–22 (2016).
- Gilbert, A. et al. Intramolecular isotopic evidence for bacterial oxidation of propane in subsurface natural gas reservoirs. *Proc. Natl Acad. Sci. USA* **116**, 6653–6658 (2019).

46. Yung, Y. L. & DeMore, W. B. *Photochemistry of Planetary Atmospheres* (Oxford Univ. Press, 1989); <https://doi.org/10.1093/oso/9780195105018.001.0001>
47. Schmidt, J. A., Johnson, M. S. & Schinke, R. Isotope effects in N<sub>2</sub>O photolysis from first principles. *Atmos. Chem. Phys.* **11**, 8965–8975 (2011).
48. Schmidt, J. A. et al. OCS photolytic isotope effects from first principles: sulfur and carbon isotopes, temperature dependence, and implications for the stratosphere. *Atmos. Chem. Phys.* **13**, 1511–1520 (2013).
49. Smith, M. D. et al. *The Atmosphere and Climate of Mars* (eds Haberle, R. M. et al.) 42–75 (Cambridge Univ. Press, 2017); <https://doi.org/10.1017/9781139060172>
50. Sneep, M. & Ubachs, W. Direct measurement of the Rayleigh scattering cross-section in various gases. *J. Quant. Spectrosc. Radiat. Transfer* **92**, 293–310 (2005).
51. Leshin, L. A., Epstein, S. & Stolper, E. M. Hydrogen isotope geochemistry of SNC meteorites. *Geochim. Cosmochim. Acta* **60**, 2635 (1996).
52. McSween, H. Y. What we learned about Mars from the SNC meteorites. *Meteoritics* **29**, 757 (1994).
53. Nyquist, L. E. et al. Age and geological history of Martian meteorites. *Space Sci. Rev.* **96**, 105–164 (2001).
54. Usui, T., Sanborn, M., Wadhwa, M. & McSween, H. Y. Jr. Petrology and trace element geochemistry of Robert Massif O4261 and O4262 meteorites, the first examples of geochemically enriched Iherzolitic shergottites. *Geochim. Cosmochim. Acta* **74**, 7283 (2010).
55. Treiman, A. H. Petrographic history of Martian meteorite ALH84001: two shocks and an ancient age. *Meteoritics* **30**, 294 (1995).
56. Mittlefehldt, D. W. ALH 84001, a cumulate orthopyroxenite member of the Martian meteorite clan. *Meteoritics* **29**, 214 (1994).
57. Borg, L. E. et al. Age of carbonates in Martian meteorite ALH84001. *Science* **286**, 90–94 (1999).
58. Lapen, T. J. et al. A younger age for ALH84001 and its geochemical link to shergottite sources on Mars. *Science* **328**, 347–351 (2010).
59. Niles, P. B., Zolotov, M. Y. & Leshin, L. A. Insights into the formation of Fe- and Mg-rich aqueous solutions on early Mars provided by ALH 84001 carbonates. *Earth Planet. Sci. Lett.* **286**, 122–130 (2009).
60. Eiler, J. M., Valley, J. W., Graham, C. M. & Fournelle, J. Two populations of carbonate in ALH84001: geochemical evidence for discrimination and genesis. *Geochim. Cosmochim. Acta* **66**, 1285–1303 (2002).
61. Valley, J. W. et al. Low-temperature carbonate concretions in the Martian meteorite ALH84001: evidence from stable isotopes and mineralogy. *Science* **275**, 1633–1638 (1997).
62. Leshin, L. A., McKeegan, K. D., Carpenter, P. K. & Harvey, R. P. Oxygen isotopic constraints on the genesis of carbonates from Martian meteorite ALH84001. *Geochim. Cosmochim. Acta* **62**, 3 (1998).
63. Holland, G., Saxton, J., Lyon, I. & Turner, G. Negative  $\delta^{18}\text{O}$  values in Allan Hills 84001 carbonate: possible evidence for water precipitation on Mars. *Geochim. Cosmochim. Acta* **69**, 1359 (2005).
64. Farquhar, J., Thiemens, M. H. & Jackson, T. Atmosphere–surface interactions on Mars:  $\Delta^{17}\text{O}$  measurements of carbonate from ALH 84001. *Science* **280**, 1580 (1998).
65. Corrigan, C. M. & Harvey, R. P. Multigenerational carbonate assemblages in Martian meteorite Allan Hills 84001: implications for nucleation, growth, and alteration. *Meteorit. Planet. Sci.* **39**, 17–30 (2004).
66. Harvey, R. P. & McSween, H. Y. Jr. A possible high-temperature origin for carbonates in the Martian meteorite ALH84001. *Nature* **382**, 49 (1996).
67. Warren, P. H. Petrologic evidence for low-temperature, possibly flood evaporitic origin of carbonates in the ALH 84001 meteorite. *J. Geophys. Res. Planets* **103**, 16759 (1998).
68. Romanek, C. S. et al. Record of fluid–rock interactions on Mars from meteorite ALH84001. *Nature* **372**, 655–657 (1994).
69. Isambert, A. et al. Magnetite-like nanocrystals formed by laser-driven shocks in siderite. *Earth Planet. Sci. Lett.* **243**, 3–4 (2006).
70. Bell, M. S. Experimental shock decomposition of siderite and the origin of magnetite in the Martian meteorite ALH 84001. *Meteorit. Planet. Sci.* **42**, 935 (2007).
71. Deines, P., Langmuir, D. & Harmon, R. S. Stable carbon isotope ratios and the existence of a gas phase in the evolution of carbonate groundwater. *Geochim. Cosmochim. Acta* **38**, 1147–1164 (1974).
72. Wen, J. S., Pinto, J. P. & Yung, Y. L. Photochemistry of CO and H<sub>2</sub>O: analysis of laboratory experiments and applications to the prebiotic Earth’s atmosphere. *J. Geophys. Res.* **94**, 14957–14970 (1989).
73. McGlynn, S. E. et al. Hydrogenation reactions of carbon on Earth: linking methane, margarine, and life. *Am. Mineral.* **105**, 599–608 (2020).
74. Koyama, S. et al. Atmospheric formaldehyde production on early Mars leading to a potential formation of bio-important molecules. *Sci. Rep.* **14**, 2397 (2024).
75. Watanabe, Y. & Ozaki, K. Relative abundance of CO<sub>2</sub>, CO and CH<sub>4</sub> in atmospheres of Earth-like lifeless planets. *Astrophys. J.* **961**, 1 (2024).
76. Feilberg, K. L., Johnson, M. S. & Nielsen, C. J. Relative rates of reaction of <sup>13</sup>C<sup>16</sup>O, <sup>12</sup>C<sup>18</sup>O, <sup>12</sup>C<sup>17</sup>O and <sup>13</sup>C<sup>18</sup>O with OH and OD radicals. *Phys. Chem. Chem. Phys.* **7**, 2318–2323 (2005).
77. Burkholder, J. B. et al. *Chemical Kinetics and Photochemical Data for Use in Atmospheric Studies, Evaluation 19* JPL Publication 19-5 (Jet Propulsion Laboratory, 2019).
78. Ueno, Y. et al. Source data for Ueno et al. ‘Synthesis of <sup>13</sup>C-depleted organic matter from CO in a reducing early Martian atmosphere’. *Figshare* <https://doi.org/10.6084/m9.figshare.25498981> (2024).

## Acknowledgements

We thank J. Foriel for helping with the stable isotope analysis. This work was supported by Japan Society for the Promotion of Science (JSPS) Grants-in-Aid for Scientific Research (KAKENHI) grant numbers JP-17H01165 and JP-22H05151 to Y.U. and A.G.; JP-21H04513 to Y.U.; JP-19H09160 and JP-22H01290 to T.U., H.K. and Y.U. J.A.S. acknowledges funding from a Carlsberg Foundation post doctoral fellowship (CF14-0519).

## Author contributions

Y.U., J.A.S. and M.S.J. designed the study. Y.U., X.Z. and A.G. performed the UV experiment and stable isotope analyses. J.A.S. performed the theoretical calculations. Y.U., M.S.J., T.U., H.K. and S.A. interpreted the results and wrote the manuscript.

## Competing interests

The authors declare no competing interests.

## Additional information

**Extended data** is available for this paper at <https://doi.org/10.1038/s41561-024-01443-z>.

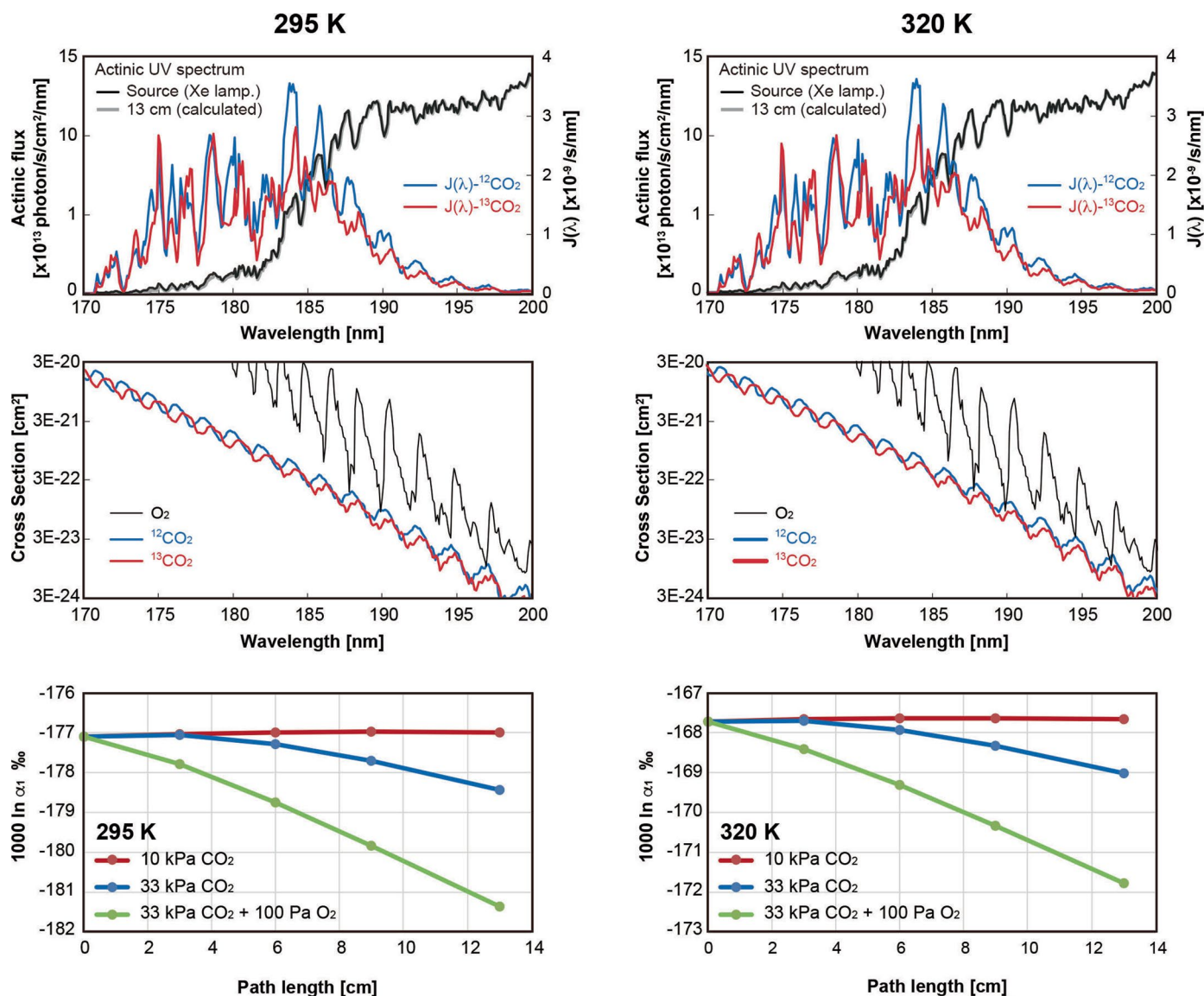
**Supplementary information** The online version contains supplementary material available at <https://doi.org/10.1038/s41561-024-01443-z>.

**Correspondence and requests for materials** should be addressed to Yuichiro Ueno.

**Peer review information** *Nature Geoscience* thanks Mao-Chang Liang and the other, anonymous, reviewer(s) for their contribution to the

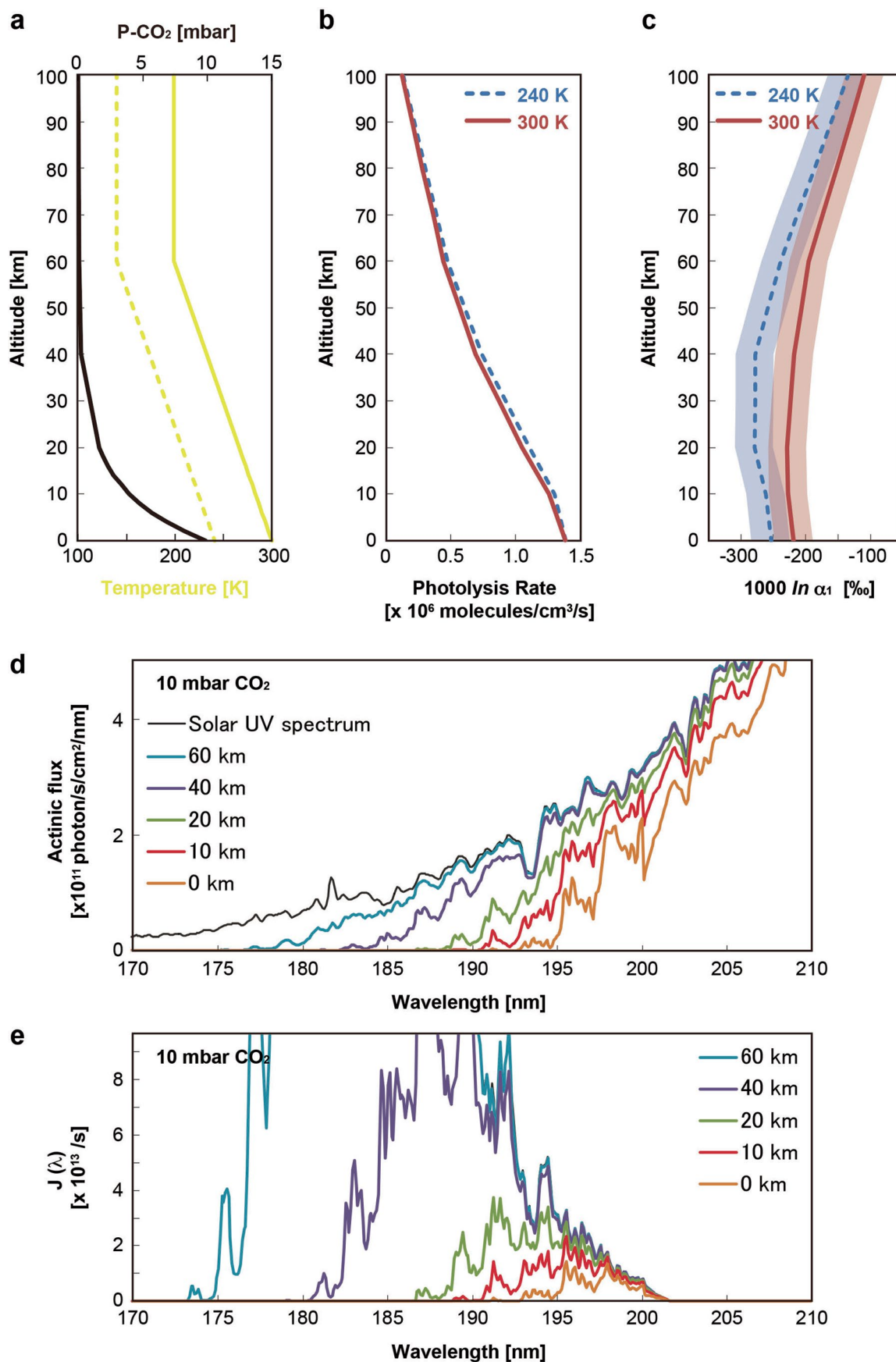
peer review of this work. Primary Handling Editor: Tamara Goldin, in collaboration with the *Nature Geoscience* team.

**Reprints and permissions information** is available at [www.nature.com/reprints](http://www.nature.com/reprints).



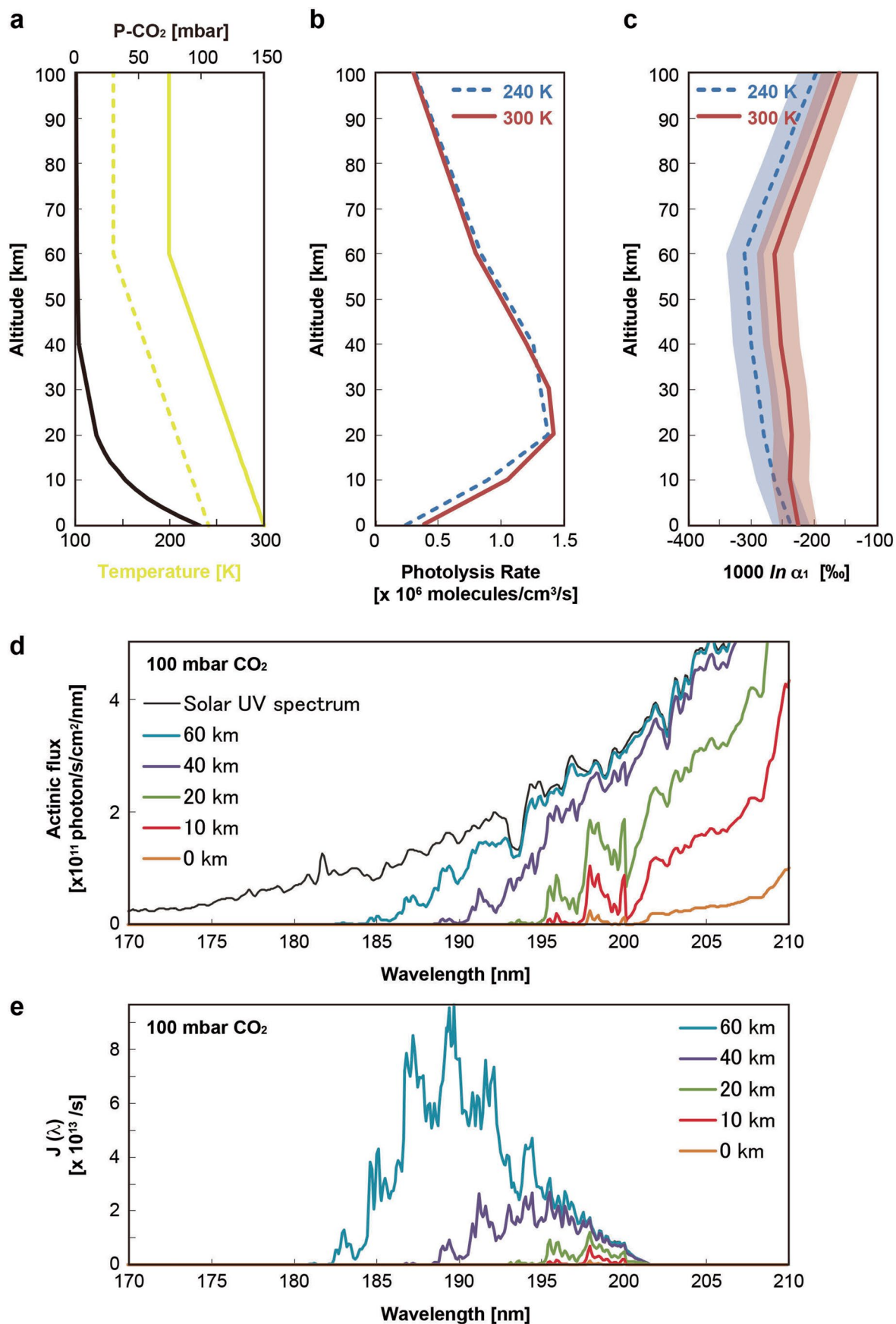
**Extended Data Fig. 1 | Calculated fractionation factors for CO<sub>2</sub> photolysis in our experimental condition. Upper panels:** Measured incident UV spectra of the Xe lamp (black) and photolysis rate coefficients (blue: <sup>12</sup>CO<sub>2</sub>, red: <sup>13</sup>CO<sub>2</sub>) showing larger isotopic fractionation accompanied by photolysis in the wavelength region longer than 183 nm. Grey lines represent actinic UV spectra calculated for shielding by 33 kPa CO<sub>2</sub> itself after an absorption path of 13 cm, which are almost identical to those of the UV source. **Middle panels:** Absorption

cross sections for <sup>12</sup>CO<sub>2</sub> (blue) and <sup>13</sup>CO<sub>2</sub> (red) calculated from first principles at 295 K (left) and 320 K (right) by Schmidt et al.<sup>17</sup> with that of O<sub>2</sub> (black) for comparison. **Bottom panels:** Estimated isotope effect (1000 ln  $\alpha_1$ ) depending on UV shielding up to a 13 cm path length in the experiment for 10 kPa CO<sub>2</sub> (red) and 33 kPa CO<sub>2</sub> (blue) (see Method). The case when 100 Pa O<sub>2</sub> was added to 33 kPa CO<sub>2</sub> is also shown in green.



**Extended Data Fig. 2 | Results from the early Mars atmosphere model, assuming 10 mbar  $P_{\text{CO}_2}$  at the surface.** **a.** Black and yellow lines represent assumed vertical profiles of  $P_{\text{CO}_2}$  and temperature, respectively. **b.** Vertical profile of CO<sub>2</sub> photolysis rate (reaction R1). **c.** Calculated isotope effect ( $1000 \ln \alpha_1$ ) of

the CO<sub>2</sub> photolysis. The red and blue lines show the results assuming surface temperatures of 300 and 240 K, respectively. The shaded area represents the uncertainty of the calculation (see Method). **d.** Calculated actinic UV spectrum at each altitude. **e.**  $J(\lambda)$  values calculated for each altitude.



**Extended Data Fig. 3 | Results from the early Mars atmosphere model, assuming 100 mbar  $P_{\text{CO}_2}$  at the surface.** **a.** Black and yellow lines represent assumed vertical profiles of  $P_{\text{CO}_2}$  and temperature, respectively. **b.** Vertical profile of CO<sub>2</sub> photolysis rate (reaction R1). **c.** Calculated isotope effect ( $1000 \ln \alpha_1$ ) of

the CO<sub>2</sub> photolysis. The red and blue lines show the results assuming surface temperatures of 300 and 240 K, respectively. The shaded area represents the uncertainty of the calculation (see Method). **d.** Calculated actinic UV spectrum at each altitude. **e.**  $J(\lambda)$  values calculated for each altitude.

**Extended Data Table 1 | Results from the CO<sub>2</sub> photolysis experiment**

ID	Irradiation time (min.)	Total Pressure (Pa)	CO <sub>2</sub> in chamber (μmol)	CO in chamber (μmol)	CO fraction	δ <sup>13</sup> C-CO ‰
33kPaCO2_0min	0	33050	5981	0.0		
33kPaCO2_15min	15	32486	5879	1.9	0.0003	-129.3
33kPaCO2_45min	45	31932	5779	5.1	0.0009	-130.4
33kPaCO2_90min	90	31388	5680	8.3	0.0015	-131.8
33kPaCO2_130min	130	30853	5583	10.3	0.0018	-131.8
33kPaCO2_200min	200	30326	5488	12.7	0.0023	-133.4
33kPaCO2 40min after lamp off		29809	5395	11.7	0.0022	-133.2
10kPaCO2_0h						
10kPaCO2_4h-1	0	9750	1764	0.0		
10kPaCO2_4h-2	240	9584	1734	5.2	0.0030	-121.4
10kPaCO2_ 24h after lamp off	240	9420	1705	5.5	0.0032	-122.1
		9260	1676	5.0	0.0030	-121.7

Results from the CO<sub>2</sub> photolysis experiment. The total pressure was decreased by removing 1.7% of the gas from the chamber from each sample aliquot. The CO fraction is the yield of product CO relative to the initial CO<sub>2</sub>, which is corrected for the decrease in total pressure by sampling. The isotopic compositions were reported as follows: δ<sup>13</sup>C - CO = (<sup>13</sup>R<sub>CO</sub>/<sup>13</sup>R<sub>CO2</sub> - 1) × 1000‰ where <sup>13</sup>R<sub>CO</sub> and <sup>13</sup>R<sub>CO2</sub> represent <sup>13</sup>C/<sup>12</sup>C ratios of CO product and initial CO<sub>2</sub>, respectively.

## Extended Data Table 2 | Results from the photochemical experiment

ID	Irradiation time (min.)	Total Pressure (Pa)	O <sub>2</sub> in chamber (μmol)	CO in chamber (μmol)	CO fraction	δ <sup>13</sup> C ‰
CO+O2_0min	0	48213	1663	805	8.44	+18.9
CO+O2_15min	15	47474		924	9.71	+16.4
CO+O2_30min	30	46746		836	9.00	+17.3
CO+O2_60min	60	46030		844	9.20	+16.1
CO+O2_90min	90	45324		577	6.57	+10.6
CO+O2_110min	110	44629		733	8.32	+18.6
CO+O2_315min	315	43945		578	6.78	+7.3
CO+O2_345min	345	43272		562	6.70	+20.0

Results from the photochemical experiment. Initially, a 1:2:8 mixture of CO, O<sub>2</sub>, and N<sub>2</sub> was photolyzed using the same UV source as in the experiments shown in Table 1. δ<sup>13</sup>C denotes the carbon isotopic composition of CO normalized against the VPDB.